50th 3AF International Conference
on Applied Aerodynamics
30 March – 1 April 2015. Toulouse, France

FP09-2015-sartor

MACH NUMBER EFFECTS ON BUFFETING FLOW ON A HALF WING-BODY CONFIGURATION

Fulvio Sartor(1) and Sebastian Timme(2)
(1) Research Associate, University of Liverpool, L69 3GH, United Kingdom. fulvio.sartor@liverpool.ac.uk
(2) Lecturer, University of Liverpool, L69 3GH, United Kingdom. sebastian.timme@liverpool.ac.uk

Abstract

A numerical study of the flow over a wing representative of a large civil aircraft at cruise condition is discussed. Reynolds-averaged Navier-Stokes simulations are conducted on a half wing-body configuration, at different Mach numbers and angles of attack. For small angles, the shock-induced separation is limited and the simulations converge towards a steady state. For each Mach number, a critical angle of attack exists where the separated region increases in size and begins to oscillate. This phenomenon, known as transonic shock buffet, is reproduced by the unsteady simulation and much information can be extracted analysing location, amplitude and frequency content of the unsteadiness.

1. INTRODUCTION

At cruise condition, the flow around a typical passenger aircraft is characterised by the presence of shock waves, interacting with the boundary layers developing over the wings [13]. A strong interaction can cause the occurrence of large scale unsteadiness such as high-amplitude self-sustained shock movements, which arise for combinations of Mach number and angle of attack [23]. This phenomenon has a significant influence on the aircraft performance and has thus been the subject of numerous studies in the past [12]. Shock buffet can be observed both in two- and three-dimensional configurations, from simple aerofoils to swept wings. In the two-dimensional case, the unsteadiness is characterised by self-sustained harmonic shock motions. It has been documented by means of experimental [20, 22, 25, 26, 37] and numerical [2, 4, 16, 18, 38] investigations. Recently, high-fidelity approaches such as zonal detached-eddy simulation (Zonal DES) [10] have thoroughly described the physics of the flow. From a more fundamental point of view, stability analysis has shown a link between the appearance of shock unsteadiness and the presence of an unstable global mode [9, 34].

When considering more complex configurations, such as a wing representative of a large civil aircraft, the unsteady behaviour presents some differences compared to the two-dimensional case [3]. The literature is more limited and does not agree on the type of shock motions. Some authors have shown that the frequency spectrum has a distinct peak [14], especially when considering wings with small sweep angle [19]. On the contrary, other studies indicate that the shock movements are broadband [5, 30]. In wind-tunnel tests, where the aeroelastic behaviour of the model must be taken into account [36], some authors have reported very broadband pressure spectra in the vicinity of the separated zone [27], while others have documented narrow peaks in the spectrum of shock location [8].

In the last decade, several numerical studies have tried to describe the complex shock motions that characterise three-dimensional buffet on a complete wing. Reynolds-averaged Navier-Stokes (RANS) approaches indicated that the buffet onset can either be predicted by the presence of massive boundary layer separation [28] or by the pressure rise at the trailing edge [31]. Limited results have been produced by URANS simulations [32], and some authors have argued that a URANS approach is not adapted to reproduce this phenomenon [6]. However, shock motions occur at much longer time scales than those of the wall-bounded turbulence, so that an unsteady RANS approach is justified. In this respect, recent studies have presented the capability of URANS to simulate transonic tail buffet [17] and the shock motions on simple three-dimensional configurations [19].

The aim of the present paper is thus to describe the transonic flow on a half wing-body configuration by means of RANS and URANS simulations. The work focuses on the characterisation of buffet unsteadiness and its onset. It is shown how time-accurate simulations can be used to gain information about the shock motions and their behaviour when considering flows at different Mach numbers.

2. NUMERICAL APPROACH

The simulations are performed using the unstructured finite volume solver DLR-TAU. The central scheme is used for the convective fluxes of the mean flow equations, and a first order Roe scheme for those of the turbulence model. Convergence is achieved using local time stepping and an implicit Backward Euler solver with an LU-SGS (Lower-Upper Symmetric Gauss-Seidel) scheme. Time-accurate computations additionally use the standard dual-time stepping approach. A previous study focussing on a single Mach number was carried out in [35] to investigate the turbulence-model dependency. In the present work, two turbulence models are considered: the negative Spalart-Allmaras (SA) [1] and an explicit algebraic Reynolds stress model in the form of Realizable Quadratic Eddy Viscosity Model (RQEVM) [33]. The main difference between the models is in the prediction of the separated zone, which plays a central role in the onset of the buffet instability.

The half wing-body configuration, chosen as test case, is shown in Fig. 1. The wing is twisted, tapered and has a constant sweep angle of 25 deg. Laminar to turbulent transition is imposed on the lower surface at about 5% of local chord, while on the upper surface this is at about 10% outboard of the crank and at 15% inboard. The flow conditions are imposed to reproduce the aerodynamic conditions of wind-tunnel tests, not discussed in this article. The reference temperature and pressure are 266.5 K and 66 kPa, respectively. Six Mach numbers are considered, spanning from 0.74 to 0.84, and the Reynolds number, based on the aerodynamic mean chord (AMC), is 3.75 million. For each turbulence model and Mach number, approximately

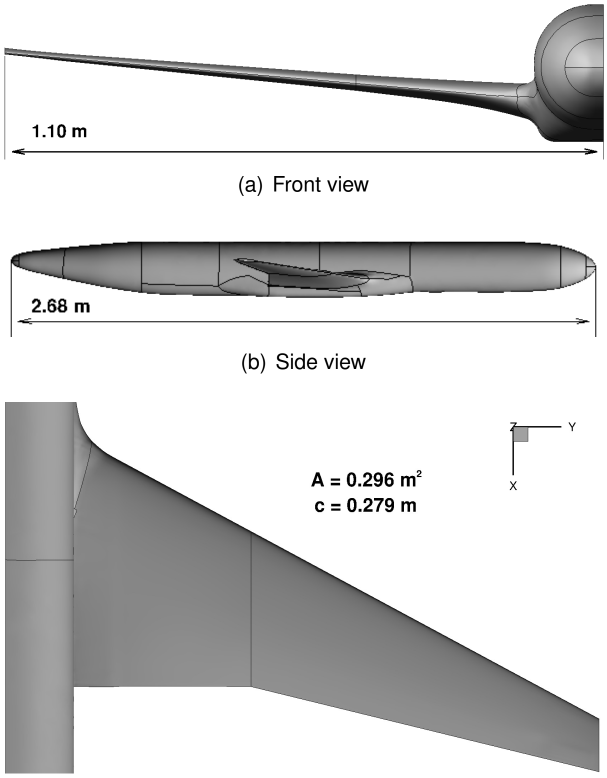

(a) Front view

(b) Side view

(c) Top view

Figure 1: RBC12 half wing-body configuration.

24 configurations are considered, where the imposed angle of attack is increased, starting from zero degrees until the buffet phenomenon is fully developed.

A family of three unstructured meshes produced using the Solar grid generator [24] has been investigated previously focussing on Mach number 0.8 [35]. After the grid dependency has been assessed, only the coarse mesh is retained for the present study. The grid, constructed using industry accepted guidelines, is composed of 2.7 million points (4.7 million elements). The initial spacing normal to all viscous walls is less than $y^+ = 0.8$, while the growth rate of cell sizes in the viscous layer is less than 1.3. The blunt trailing edge is described by 8 cells corresponding to a spacing of about 0.15% of the local chord, and a spacing of 0.5% and 0.1% of the span is imposed for the wing root and tip, respectively.

3. STEADY SIMULATIONS

In this section we discuss the steady-state solutions. In Fig. 2 the evolution of the final density residual is plotted over the angle of attack for all considered Mach numbers. When the incidence is small, the

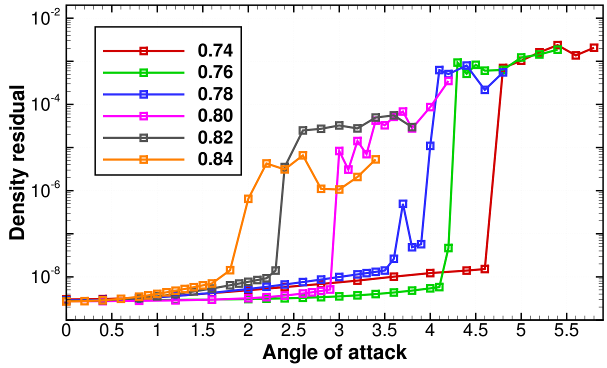

(a) SA turbulence model

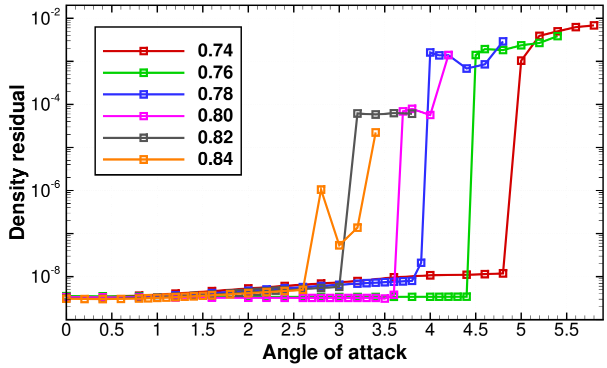

(b) RQEVM

Figure 2: Density residual vs angle of attack for different Mach numbers.

results present a good level of convergence. After a threshold, which depends on the Mach number, the final residual rises and all cases fail to converge to the specified limit. The residuals reach a plateau and further iterations do not reduce their values. In those cases the steady-state results are not reliable and a URANS simulation should be considered instead to investigate the presence of shock motions. As it will be seen in Sec. 4, the rise of the density residual is linked to the occurrence of unsteadiness. Therefore, by comparing Fig. 2a and Fig. 2b, it can be noticed that for all Mach numbers the RQEVM predicts a buffet onset for higher angles of attack. The steady-state solutions obtained with the two turbulence models are similar, even when full convergence is not achieved.

Fig. 3 presents a comparison of the drag polars at each Mach number, where it can be seen that the predicted values of lift and drag coefficients are in reasonable agreement, especially when both turbulence models converge. In both plots it can be noticed that when the Mach number is small, an abrupt change in the polar line indicates the failure to converge. This feature, also observed in other studies, is often used as an indicator of the presence of the

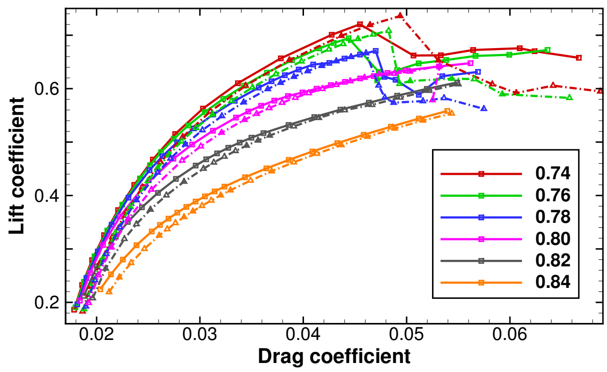

Figure 3: Drag polars. Solid line: SA turbulence model; dash-dotted line: RQEVM.

unsteadiness. In this respect, [29] showed experimentally that the distinct slope change (or kink) in the lift curve coincides with buffet onset as measured with a strain gauge on a two-dimensional aerofoil. However, when focussing on higher Mach numbers, this kink cannot be observed. For this reason, the abrupt change in the forces on the wing is probably linked to the presence of a massively separated zone, the relation of which to the unsteadiness is not straightforward to establish. In addition, when considering Mach numbers higher than 0.8, the drag polars obtained with the two turbulence models are identical, indicating similar buffet onset. However, as it will be shown in Sec. 4, this is not the case.

Another common method to predict the presence of unsteadiness and its position is to analyse the distribution of the sectional-lift coefficient along the wing span. For this purpose, the pressure coefficient of each steady-state solution is extracted along several wing sections and the contribution of this section to the total lift coefficient is extracted. Although many studies in two-dimensional configurations do not show a clear link between buffeting flow and the topology of the flow separation [9, 34], the instability onset is often determined when the separated zone reaches the trailing edge and bursts [28, 39].

The results are presented in Fig. 4 for the SA turbulence model, showing the sectional lift from the wing root to the wing tip. The presence of the crank can be noticed by a small discontinuity at 42% of the span. Since the wing is twisted, the positive washout is responsible for the decreasing lift while approaching the wing tip. For each Mach number, inboard of the crank and in its vicinity, the sectional-lift coefficients in Fig. 4 keep increasing constantly with the angle of attack. Outboard of the crank, the pressure loss due to the shock-induced separation causes an abrupt drop in the local lift. A further

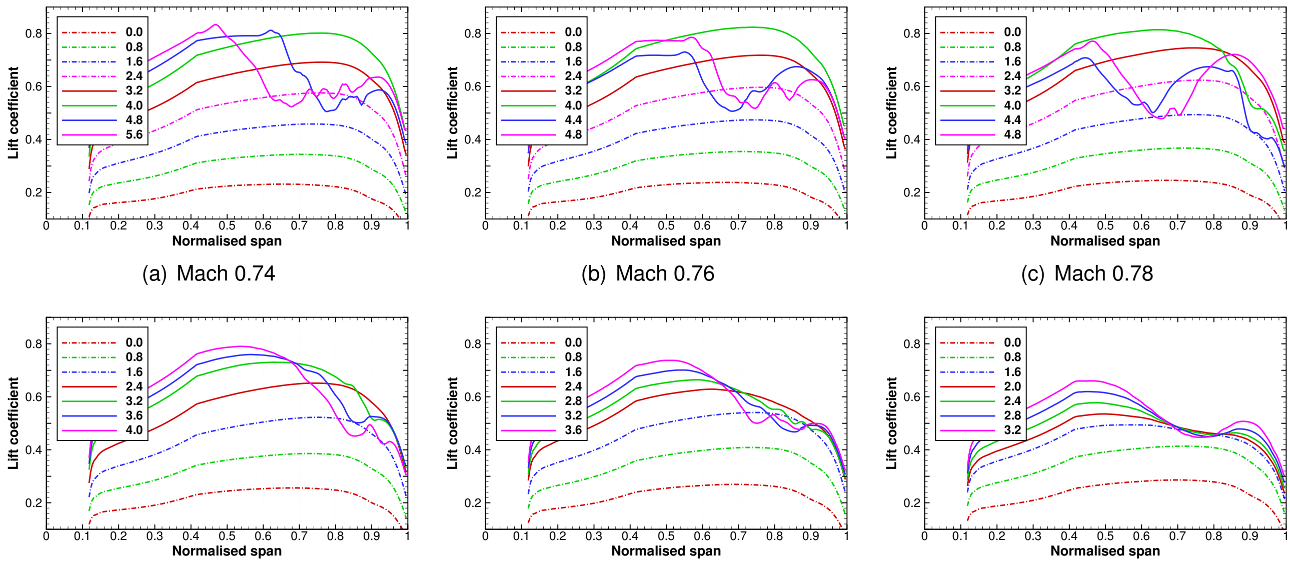

(a) Mach 0.74 (b) Mach 0.76 (c) Mach 0.78

(d) Mach 0.80 (e) Mach 0.82 (f) Mach 0.84

Figure 4: Span-wise distribution of sectional-lift coefficient for SA turbulence model.

increase in the angle of attack is responsible for a wider decrease of the sectional-lift coefficient, indicating that the recirculation zone moves towards the fuselage.

By comparing the different plots in Fig. 4, it can also be noticed that the pressure drop due to the shock-induced separation is sharper for lower Mach numbers. On the contrary, when the Mach number is 0.84 (Fig. 4f) the lift coefficient in sections around 75% of the span remains between 0.42 and 0.46 for all angles of attack greater than 1.6 deg. This indicates that the separated zone is not moving in the spanwise direction, but only increasing its chordwise extent. In this respect, the lift drop on the plot becomes larger while increasing the angle of attack.

Although not shown, similar results are obtained with RQEVM in terms of lift distribution and pressure drop when increasing the Mach number. Consistently with the previous observations, higher angles of attack are needed in this case to predict the presence of large separations. The results confirm that a link can be found between the abrupt sectional-lift decrease and the appearance of unsteadiness. However, one should bare in mind that for those angles of attack the RANS simulation does not converge, indicating the requirement of an unsteady approach.

4. UNSTEADY SIMULATIONS

The RANS results described in the previous section are now used as a starting point for unsteady computations. The time discretisation is switched to dual-time stepping and every time step is iterated until a convergence criterion is reached. The total physical time simulated is 0.09 s for each case, corresponding to approximately 30 buffet cycles. In every simulation, a transient part can be observed, where the flow builds up the unsteadiness. Once this transient has passed, time histories of force and moment coefficients, as well as the mean and standard deviation of all flow variables are recorded. A total of 50 and 40 cases have been time-accurately simulated for SA and RQEVM, respectively. Each case is obtained in roughly two weeks using 48 cores of Intel Xeon X5660 processors.

For an unsteady simulation, a time-step size has to be chosen depending on the time scale of the flow unsteadiness. A convergence study has been carried out in [35] for Mach number 0.8, concluding that the time step must be smaller than 5 μs. Since the convergence study has been carried out for one particular configuration, the time-step size chosen for all URANS simulations is 2 μs. This precaution has been taken to prevent inaccuracy in case the buffet frequency is significantly higher for some combination of angle of attack and Mach number. This value is almost three orders of magnitude smaller than the convective time, defined by the AMC and reference velocity, which for this case is around 10^{-3} s. Finally, it has to be considered that the shock-induced separated zone changes its size during a buffet cycle, depending on the shock position. Instead of performing a fixed number of iterations per time step, a Cauchy convergence criterion is applied. Hence,

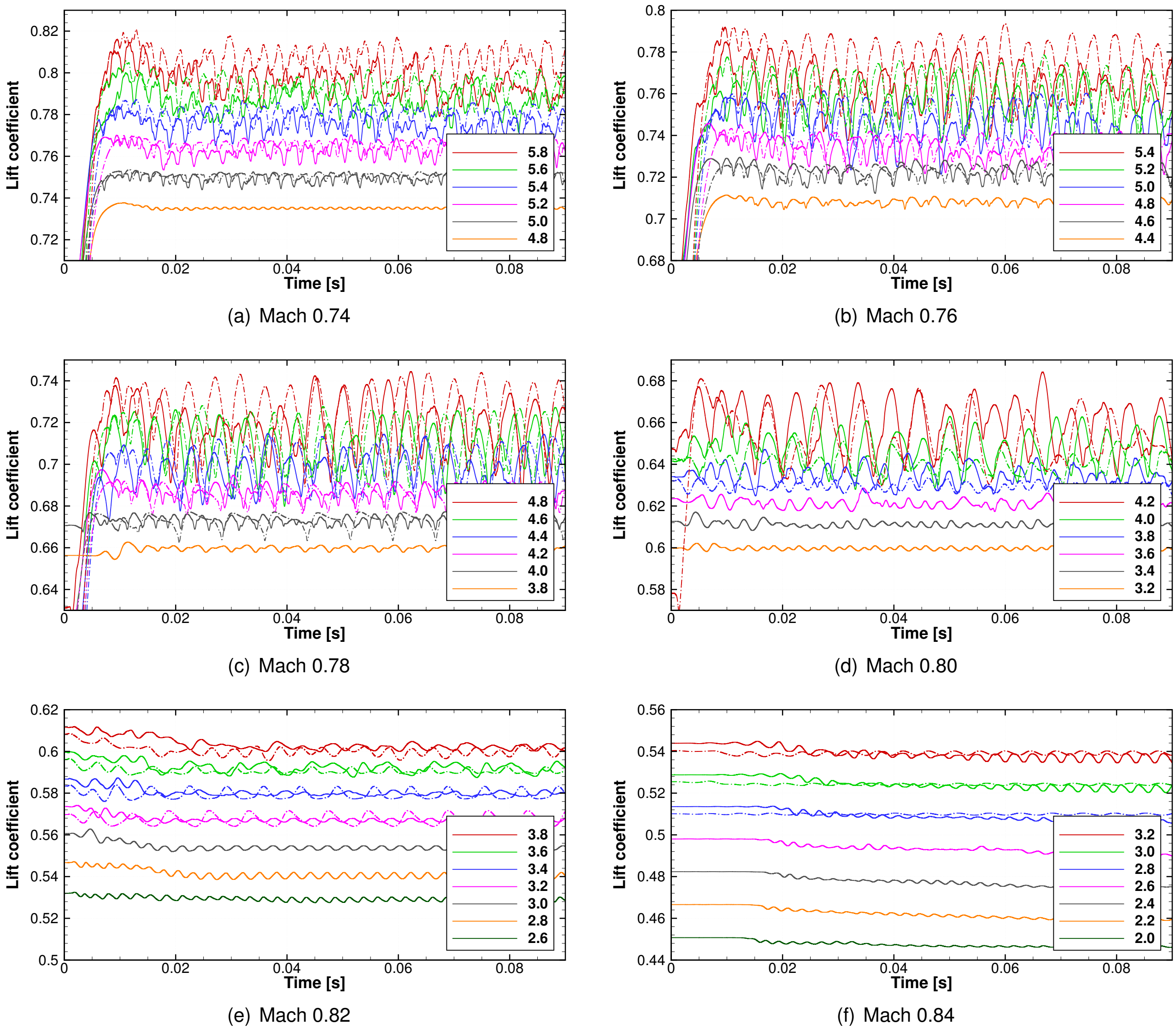

(a) Mach 0.74
(b) Mach 0.76
(c) Mach 0.78
(d) Mach 0.80
(e) Mach 0.82
(f) Mach 0.84

Figure 5: Time history of lift coefficients. Solid line: SA turbulence model; dash-dotted line: RQEVM.

each time step is iterated until the drag coefficient in the last 20 inner iterations shows a relative error smaller than 10^{-8}. This criterion results in more inner iterations when in presence of a massive separation and fewer when the flow is easily converged.

A wide range of angles of attack is now considered for each Mach number and both turbulence models introduced in Sec. 3. Fig. 5 presents the time evolution of the lift coefficient, where each plot is referred to a given Mach number. It can be seen that up to 0.02 s are needed for the flow to establish the fully developed shock buffeting regime. When the Mach number is high, the lift coefficient does not diverge significantly from its steady-state value. Focussing on Mach numbers 0.74 to 0.78 on the other hand, the time-average of the unsteady simulation is not close to the flow field predicted by the steady approach. Comparing with Fig. 3, it can be concluded that a sudden change in the wing loads (or a kink in the drag polars) is not an indicator of the presence of unsteady flow, as suggested in [15], but only a consequence of the failure of the RANS simulation to converge to a steady state close to the time average of the unsteady flow.

The solid lines in Fig. 5 have been obtained using SA turbulence model, while the dash-dotted refer to the RQEVM. For all cases, a satisfying agreement is observed when comparing average value and amplitude of the fluctuations. The main difference between the two models is the onset. The critical value of the angle of attack is smaller for SA. In addition, close to the onset, this model predicts fluctuations which have a simple frequency content. This feature is not observed in the RQEVM, where even for

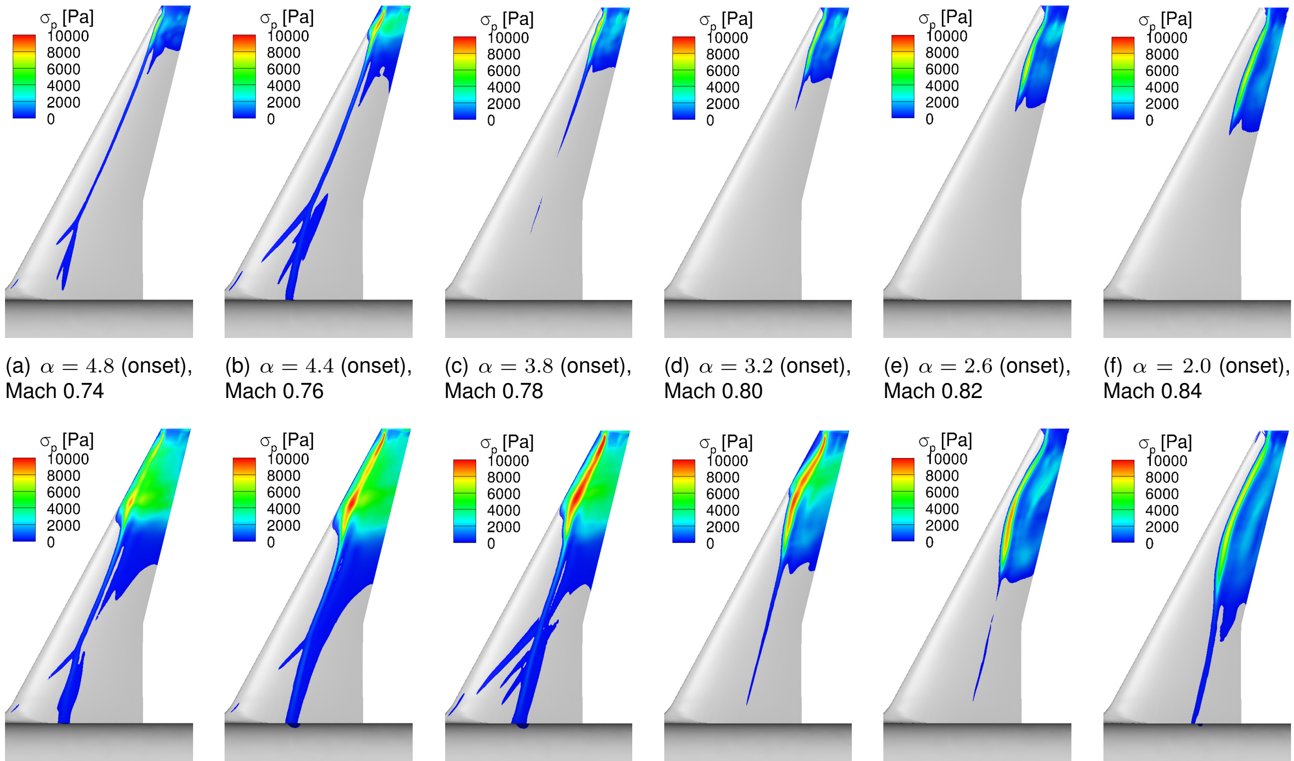

(a) $\alpha = 4.8$ (onset), Mach 0.74
(b) $\alpha = 4.4$ (onset), Mach 0.76
(c) $\alpha = 3.8$ (onset), Mach 0.78
(d) $\alpha = 3.2$ (onset), Mach 0.80
(e) $\alpha = 2.6$ (onset), Mach 0.82
(f) $\alpha = 2.0$ (onset), Mach 0.84
(g) $\alpha = 5.4$ (buffet), Mach 0.74
(h) $\alpha = 5.0$ (buffet), Mach 0.76
(i) $\alpha = 4.4$ (buffet), Mach 0.78
(j) $\alpha = 3.8$ (buffet), Mach 0.80
(k) $\alpha = 3.2$ (buffet), Mach 0.82
(l) $\alpha = 2.8$ (buffet), Mach 0.84

Figure 6: Standard deviation of pressure at onset condition and when unsteadiness is fully developed.

small angles of attack the shock motions are not periodic. This feature will be discussed in more details when analysing the frequency content of the signals. By comparing results obtained with different Mach numbers, it can be observed that the onset occurs at smaller angles of attack when increasing the Mach number, as observed in two-dimensional flows [26]. Then, when unsteadiness occurs, the average value of the lift is smaller (note that the vertical axis is adjusted in each plot), and also the amplitude of the fluctuations is more limited (the scale does not change in the plots).

During the unsteady simulations the variance of the fluctuating pressure is computed. This quantity gives access to the spatial distribution of the unsteady part of the flow. Fig. 6 presents the pressure standard deviation σ_p, evaluated at the surface of the wing for all Mach numbers, at onset conditions (Figs. 6a through 6f) and when the buffet is developed (Fig. 6g through 6l). Only the results obtained with SA turbulence model are discussed. When the angles of attack are small, the shock trace lays on a straight line, in between the leading and trailing edge. The unsteady separated zone is only in the wing-tip region. For all Mach numbers, the unsteady zones grows bigger with increasing angle of attack, and the centre of the unsteadiness moves towards the fuselage, in agreement with [37]. In addition, the shock trace bends (Fig. 6i) or even adopts a serpentine shape (Fig. 6k).

Comparing all cases, it can be noticed that when the Mach number is small the separated zone is more limited, but the whole shock foot is unsteady. This occurs regardless the presence of separation, also inboard of the crank and already from onset. For some cases the shock foot is unsteady even on the fuselage (Fig. 6a and Fig. 6b). On the contrary when focussing on cases with the highest Mach number, no unsteady flow can be found on the leading edge, even when the unsteadiness is fully developed (Fig. 6k and Fig. 6l). Overall, very similar shock-foot traces have been observed in numerical studies on a tapered and swept wing [5], non-tapered swept configuration [19], and experimental investigations [37].

The time histories of the lift coefficient are now analysed. As pointed out in [11], numerical signals issued from CFD are often oversampled and have a short duration. To overcome the problem of the limited spectrum definition we used an autoregressive estimator [21], rather than a traditional Fast Fourier Transform. Following the steps of [10],

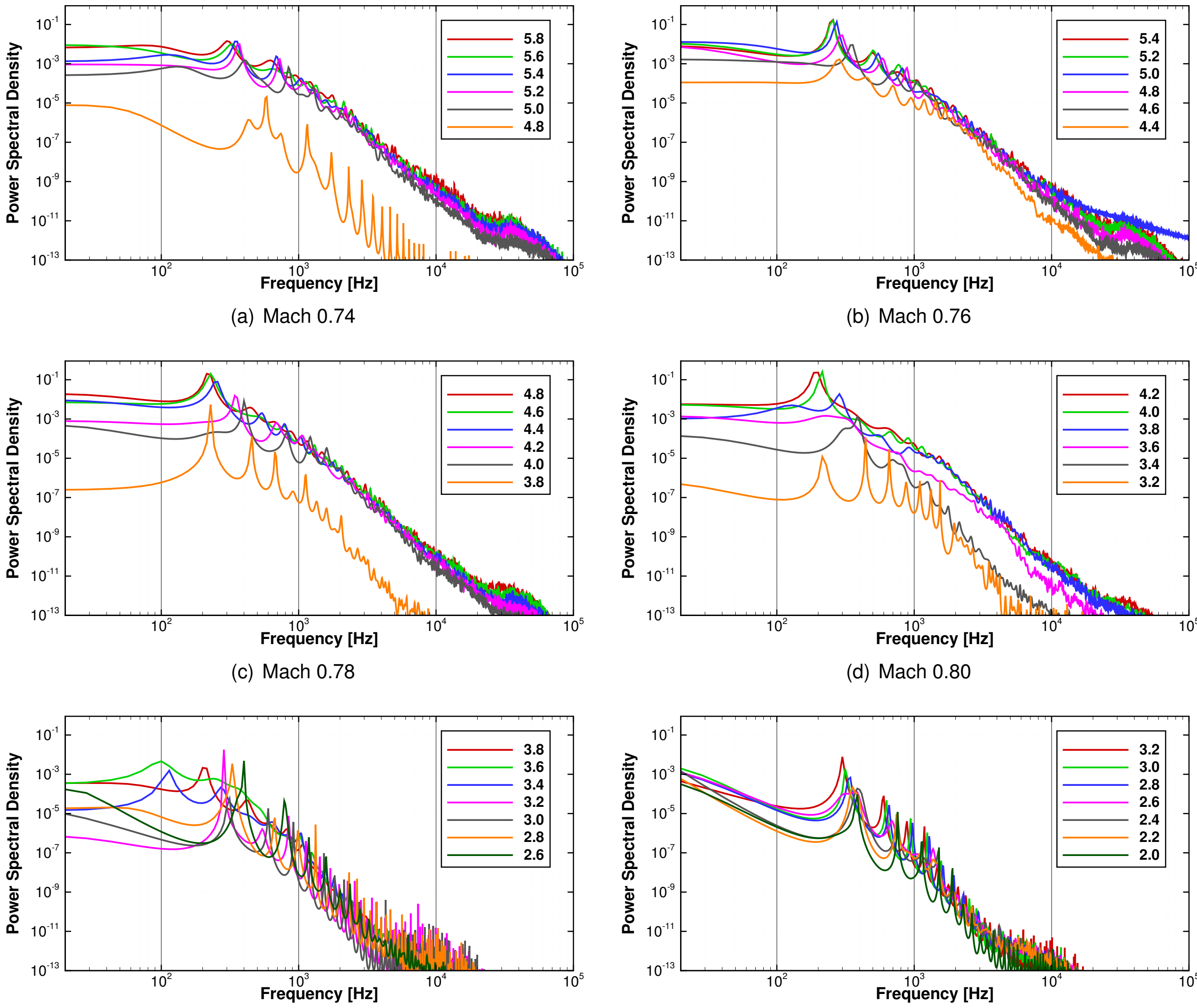

(a) Mach 0.74

(b) Mach 0.76

(c) Mach 0.78

(d) Mach 0.80

(e) Mach 0.82

(f) Mach 0.84

Figure 7: Power Spectral Density of lift coefficients for SA turbulence model.

the power spectral density (PSD) is computed using Burg's method [7]. Each case is analysed using a single window covering the total duration of the lift signal without the initial transient. The results are presented in Fig. 7 for the SA turbulence model.

In all plots it can be seen that for small angles of attack the PSD seems to be characterised by a narrowband frequency content. At onset condition, the signals are not only periodic, but also characterised by a single-frequency harmonic motion. For example, at Mach 0.78 (Fig. 7c) the onset condition occurs at narrowband frequency, with a distinguish peak centred at 220 Hz. The presence of these periodic motions can be noticed also in Fig. 5. When increasing the angle of attack, the lift signal presents greater shock motions and as a consequence the peak in the PSD is more energetic. A further increase in the angle of attack is responsible for this peak to move towards lower frequency and to become wider. The shock unsteadiness is now characterised by non-periodic motions. This behaviour is visible in all plots of Fig. 7. When focussing on the highest Mach numbers, the peaks are generally more narrow, which is consistent with the observations in the time-histories of the lift coefficient. In addition, the energy contained in the unsteadiness is lower for those cases.

When considering the RQEVM, not shown in the plot, a similar behaviour can be observed when comparing cases with the same flow condition. The onset occurs at a higher angle of attack and with a frequency content characterised by broadband unsteadiness from the beginning of the oscillations. Overall, shock motions occur around 100 to

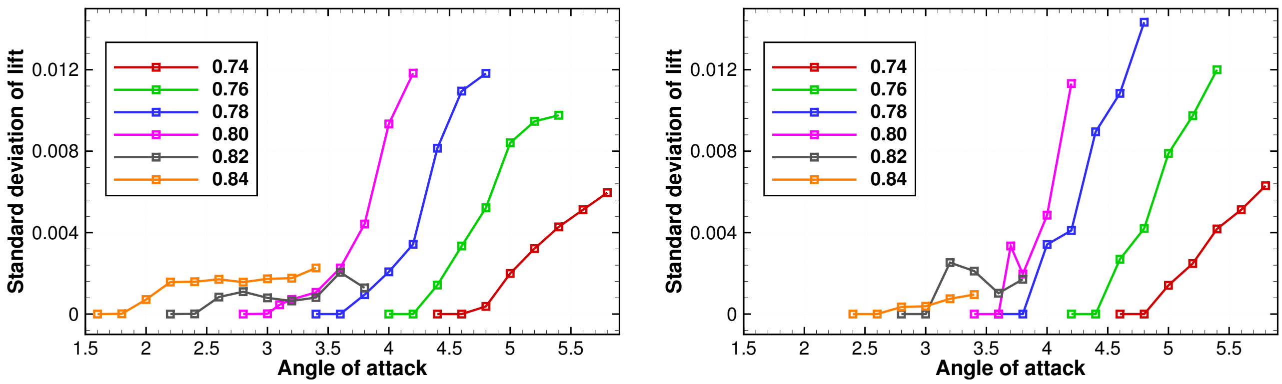

(a) SA turbulence model

(b) RQEVM

Figure 8: Standard deviation of lift coefficient vs angle of attack for different Mach numbers.

400 Hz. This corresponds, when scaled by a non-dimensional frequency given by the inverse of the convective time, to a Strouhal number of about 0.1 to 0.4. Similar values have been found in the experimental investigation of [37] on the Nasa Common Research Model at similar flow conditions, or in [5] by means of Zonal DES.

Fig. 8 summarises the major results in terms of unsteadiness for all the Mach numbers at all angles of attack. Each symbol has been obtained by computing the standard deviation of the lift coefficient in a time-accurate simulation, once the transient has passed. A zero standard deviation indicates the absence of unsteadiness in the flow, while high values describe large shock motions. By comparing Fig. 8a with Fig. 8b it can be seen that the RQEVM predicts an onset of the unsteadiness for greater angles of attack. Then, similar values of the standard deviation are observed. The unsteady content is more distinct for low Mach numbers, and the magnitude of unsteadiness keeps increasing with the angle of attack (for all cases considered). For higher Mach numbers, the magnitude of unsteadiness reaches a plateau, which is particularly visible for RQEVM.

5. CONCLUSIONS

The flow over a typical large transport aircraft at cruise conditions has been analysed using a half wing-body model. Steady-state solutions converge only when the flow does not present a large separated zone on the upper surface of the wing. Then, time-accurate simulations have to be considered. It has been shown that for all Mach numbers, when considering small angles of attack, the shock-induced separation has a limited size and the flow is steady. Increasing the angle of attack, the separated zone close to the wing tip begins to oscillate and the unsteadiness moves towards the fuselage. An increasingly broadband frequency content can be observed, while the most energetic frequency in the PSD decreases.

Comparing the buffet phenomenon at different Mach numbers, the onset of the unsteadiness occurs for smaller angles of attack when increasing the Mach number. Similar frequency content is then observed for different cases. Focusing on the magnitude of the unsteadiness, the standard deviation of the lift is lower for high Mach numbers, and reaches a plateau immediately after the onset. In these cases, only the separated zone is unsteady. For lower Mach numbers, although the separated zone has a reduced size, the unsteadiness can be observed on the entire upper surface of the wing. The amplitude of the shock motions increase constantly when increasing the angle of attack.

The high number of cases presented in this study allows the creation of a database which, to the authors' knowledge, has not been documented in literature before. Previous studies were able to compare flow conditions at different angles of attack only for two-dimensional cases. More realistic studies on half-wing body configurations were limited to few angles of attack and one Mach number. The results presented indicate that, while high-fidelity approaches can improve the quality of the results, the URANS approach is capable of describing the main features of the buffet phenomenon.

Acknowledgments

The research leading to these results has received funding from the European Union's Seventh Framework Programme (FP7/2007-2013) for the Clean Sky Joint Technology Initiative under grant agreement n° 336948.

REFERENCES

[1] S. R. Allmaras and F. T. Johnson. Modifications and clarifications for the implementation of the Spalart-Allmaras turbulence model. In *ICCFD7-1902, 7th International Conference on Computational Fluid Dynamics, Big Island, Hawaii*, 2012.

[2] G. Barakos and D. Drikakis. Numerical simulation of transonic buffet flows using various turbulence closures. *International Journal of Heat and Fluid Flow*, 21(5):620–626, 2000.

[3] B. Benoit and I. Legrain. Buffeting prediction for transport aircraft applications based on unsteady pressure measurements. *AIAA Paper 87–2356*, 1987.

[4] V. Brunet. Computational study of buffet phenomenon with URANS equations. *AIAA Paper 2003–3679*, 2003.

[5] V. Brunet and S. Deck. Zonal-detached eddy simulation of transonic buffet on a civil aircraft type configuration. In *Advances in Hybrid RANS-LES Modelling*, pages 182–191. Springer, 2008.

[6] V. Brunet and S. Deck. Zonal-detached eddy simulation of transonic buffet on a civil aircraft type configuration. *AIAA Paper 2008–4152*, 2008.

[7] J. P. Burg. Maximum entropy spectral analysis. In *Modern Spectrum Analysis*, pages 34–41. Edited by D. G. Childers, IEEE Press, New York, 1978.

[8] D. Caruana, A. Mignosi, M. Corrègeand, A. Le Pourhiet, and A. M. Rodde. Buffet and buffeting control in transonic flow. *Aerospace science and technology*, 9(7):605–616, 2005.

[9] J. D. Crouch, A. Garbaruk, D. Magidov, and A. Travin. Origin of transonic buffet on aerofoils. *Journal of Fluid Mechanics*, 628:357–369, 2009.

[10] S. Deck. Numerical simulation of transonic buffet over the OAT15A airfoil. *AIAA Journal*, 43(7):1556–1566, 2005.

[11] S. Deck and A. T. Nguyen. Unsteady side loads in a thrust-optimized contour nozzle at hysteresis regime. *AIAA Journal*, 42(9):1878–1888, 2004.

[12] J. Délery and J. G. Marvin. Shock-wave boundary layer interactions. *AGARDograph No. 280*, 1986.

[13] D. S. Dolling. Fifty years of shock-wave/boundary-layer interaction research: what next? *AIAA Journal*, 39(8):1517–1531, 2001.

[14] M. Farhangnia, G. P. Guruswamy, and S. Biringen. Transonic-buffet associated aeroelasticity of a supercritical wing. *AIAA Paper 96–0286*, 1996.

[15] M. Gariépy, B. Malouin, J-Y. Trépanier, and É. Laurendeau. Far-field drag decomposition applied to the drag prediction workshop 5 cases. *Journal of Aircraft*, 50(6):1822–1831, 2013.

[16] E. Goncalves and R. Houdeville. Turbulence model and numerical scheme assessment for buffet computations. *International journal for numerical methods in fluids*, 46(11):1127–1152, 2004.

[17] S. A. Illi, C. Fingskes, T. Lutz, and E. Krämer. Transonic tail buffet simulations for the common research model. *AIAA Paper 2013–2510*, 2013.

[18] M. Iovnovich and D. E. Raveh. Reynolds-Averaged Navier-Stokes study of the shock-buffet instability mechanism. *AIAA Journal*, 50(4):880–890, 2012.

[19] M. Iovnovich and D. E. Raveh. Numerical study of shock buffet on three-dimensional wings. *AIAA Journal*, 53(2):449–463, 2015.

[20] L. Jacquin, P. Molton, S. Deck, B. Maury, and D. Soulevant. Experimental study of shock oscillation over a transonic supercritical profile. *AIAA Journal*, 47(9):1985–1994, 2009.

[21] S. M. Kay and S. L. J. Marple. Spectrum analysis – a modern perspective. *Proceedings of the IEEE*, 69(11):1380–1419, 1981.

[22] B. H. K. Lee. Oscillatory shock motion caused by transonic shock boundary-layer interaction. *AIAA Journal*, 28(5):942–944, 1990.

[23] B. H. K. Lee. Self-sustained shock oscillations on airfoils at transonic speeds. *Progress in Aerospace Sciences*, 37(2):147–196, 2001.

[24] D. G. Martineau, S. Stokes, S. J. Munday, A. P. Jackson, B. J. Gribben, and N. Verhoeven.

Anisotropic hybrid mesh generation for industrial rans applications. *AIAA Paper 2006-534*, 2006.

[25] J. B. McDevitt, J. L. L. Levy, and G. S. Deiwert. Transonic flow about a thick circular-arc airfoil. *AIAA Journal*, 14(5):606–613, 1976.

[26] J. B. McDevitt and A. F. Okuno. Static and dynamic pressure measurements on a NACA 0012 airfoil in the ames high reynolds number facility. *NASA TP-2485*, 1985.

[27] P. Molton, J. Dandois, A. Lepage, V. Brunet, and R. Bur. Control of buffet phenomenon on a transonic swept wing. *AIAA Journal*, 51(4):761–772, 2013.

[28] H. H. Pearcey. A method for the prediction of the onset of buffeting and other separation effects from wind tunnel tests on rigid models. Technical report, DTIC Document, 1958.

[29] H. H. Pearcey and D. W. Holder. Simple methods for the prediction of wing buffeting resulting from bubble type separation. *Aero Rep. 1024*, 1962.

[30] J. Reneaux, V. Brunet, D. Caruana, S. Deck, and P. Naudin. A combined experimental and numerical investigation of the buffet phenomenon and its control through passive and active devices. *ONERA Tiré à Part*, 2005(103), 2005.

[31] C. L. Rumsey, D. O. Allison, R. T. Biedron, P. G. Buning, T. G. Gainer, J. H. Morrison, S. M. Rivers, S. J. Mysko, and D. P. Witkowski. Cfd sensitivity analysis of a modern civil transport near buffet-onset conditions. *NASA TM-2001-211263*, 2001.

[32] C. L. Rumsey, J. H. Morrison, and R. T. Biedron. Cfd variability for a civil transport aircraft near buffet-onset conditions. *NASA TM-2003-212149*, 2003.

[33] T. Rung, H. Lübcke, M. Franke, L. Xue, F. Thiele, and S. Fu. Assessment of explicit algebraic stress models in transonic flows. *Engineering turbulence modelling and experiments 4*, pages 659–668, 1999.

[34] F. Sartor, C. Mettot, and D. Sipp. Stability, receptivity and sensitivity analyses of buffeting transonic flow over a profile. *AIAA Journal*, pages 1–14, 2014.

[35] F. Sartor and S. Timme. Reynolds-Averaged Navier-Stokes simulations of shock buffet on half wing-body configuration. *AIAA Paper 2015–1939*, 2015.

[36] P. C. Steimle, D-C. Karhoff, and W. Schröder. Unsteady transonic flow over a transport-type swept wing. *AIAA Journal*, 50(2):399–415, 2012.

[37] Y. Sugioka, D. Numata, K. Asai, S. Koike, K. Nakakita, and S. Koga. Unsteady PSP measurement of transonic buffet on a wing. *AIAA Paper 2015–0025*, 2015.

[38] M. Thiery and E. Coustols. Numerical prediction of shock induced oscillations over a 2D airfoil: Influence of turbulence modelling and test section walls. *International Journal of Heat and Fluid Flow*, 27(4):661–670, 2006.

[39] F. Thomas and G. Redeker. *A method for calculating the transonic buffet boundary including the influence of Reynolds number*. DFVLR, 1971.